Chemical Science

ROYAL SOCIETY OF CHEMISTRY

EDGE ARTICLE

View Article Online
View Journal | View Issue

Cite this: *Chem. Sci.*, 2021, **12**, 14499

All publication charges for this article have been paid for by the Royal Society of Chemistry

Received 5th July 2021
Accepted 13th September 2021

DOI: 10.1039/d1sc03665c

rsc.li/chemical-science

Simplifying and expanding the scope of boron imidazolate framework (BIF) synthesis using mechanochemistry†

Cameron B. Lennox, [ab] Jean-Louis Do, [ab] Joshua G. Crew, [ac] Mihails Arhangelskis, [ad] Hatem M. Titi, [ab] Ashlee J. Howarth, [bef] Omar K. Farha [f] and Tomislav Friščić *[ab]

Mechanochemistry enables rapid access to boron imidazolate frameworks (BIFs), including ultralight materials based on Li and Cu(I) nodes, as well as new, previously unexplored systems based on Ag(I) nodes. Compared to solution methods, mechanochemistry is faster, provides materials with improved porosity, and replaces harsh reactants (*e.g. n*-butylithium) with simpler and safer oxides, carbonates or hydroxides. Periodic density-functional theory (DFT) calculations on polymorphic pairs of BIFs based on Li^+, Cu^+ and Ag^+ nodes reveals that heavy-atom nodes increase the stability of the open SOD-framework relative to the non-porous dia-polymorph.

Mechanochemistry[1–7] has emerged as a versatile methodology for the synthesis and discovery of advanced materials, including nanoparticle systems[8–10] and metal–organic frameworks (MOFs),[11–15] giving rise to materials that are challenging to obtain using conventional solution-based techniques.[16–18] Mechanochemical techniques such as ball milling, twin screw extrusion[19] and acoustic mixing[20,21] have simplified and advanced the synthesis of a wide range of MOFs, permitting the use of simple starting materials such as metal oxides, hydroxides or carbonates,[22,23] at room temperature and without bulk solvents, yielding products of comparable stability and, after activation, higher surface areas than solution-generated counterparts.[24–29] The efficiency of mechanochemistry in MOF synthesis was recently highlighted by accessing zeolitic imidazolate frameworks (ZIFs)[30,31] that were theoretically predicted, but not accessible under conventional solution-based conditions.[17]

The advantages of mechanochemistry in MOF chemistry led us to address the possibility of synthesizing boron imidazolate frameworks (BIFs),[32–34] an intriguing but poorly developed class of microporous materials analogous to ZIFs, comprising equimolar combinations of tetrahedrally coordinated boron(III) and monovalent Li^+ or Cu^+ cations as nodes (Fig. 1A–C). Although BIFs offer an attractive opportunity to access microporous MOFs with lower molecular weights, particularly in the case of "ultralight" systems based on Li^+ and B(III) centers, this family of materials has remained largely unexplored – potentially due

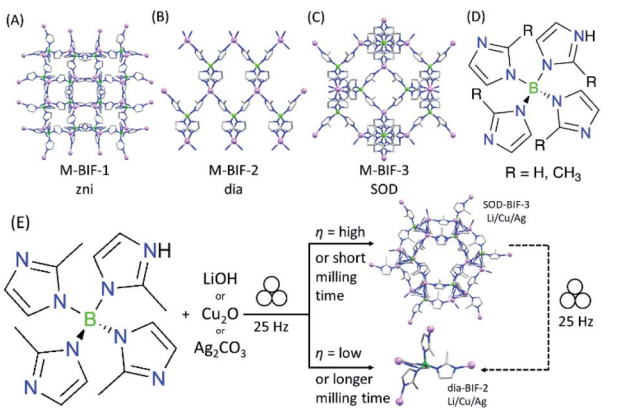

Fig. 1 Structures of previously reported BIFs with: (A) zni-, (B) dia-, or (C) SOD-topology (M = Li, Cu); (D) tetrakis(imidazolyl)boric acids used herein for mechanochemical BIF synthesis; and (E) schematic representation of the herein developed mechanosynthesis of dia- and SOD BIF polymorphs based on Li, Cu or Ag metal nodes.

[a]*Department of Chemistry, McGill University, 801 Sherbrooke St. W, H3A 0B8 Montreal, Canada. E-mail: tomislav.friscic@mcgill.ca*

[b]*FRQNT Quebec Centre for Advanced Materials (QCAM/CQMF), Montreal, Canada*

[c]*School of Chemistry, Cardiff University, Main Building. Park Place, Cardiff CF10 3AT, UK*

[d]*Faculty of Chemistry, University of Warsaw, 1 Pasteura St, 02-093 Warsaw, Poland*

[e]*Department of Biochemistry and Chemistry, Concordia University, 7141 Sherbrooke St. W, H4B 1R6 Montreal, Canada*

[f]*International Institute for Nanotechnology, Department of Chemistry, Northwestern University, 2145 Sheridan Road, 60208 Evanston, Il, USA*

† Electronic supplementary information (ESI) available: Experimental and theoretical procedures, and selected PXRD, TGA, FTIR-ATR, ICP-MS, nitrogen sorption data. Crystallographic data for BIF-2-Ag, BIF-3-Ag and [**Hamb**$^+$][B(**Meim**)$_4^-$]·2H_2O. CCDC 2081806, 2081807 and 2084944. For ESI and crystallographic data in CIF or other electronic format see DOI: 10.1039/d1sc03665c

to the need for harsh synthetic conditions, including the use of *n*-butyllithium in a solvothermal environment.[32–34]

We now show how switching to the mechanochemical environment enables lithium- and copper(I)-based BIFs to be prepared rapidly (*i.e.*, within 60–90 minutes), without elevated temperatures or bulk solvents, and from readily accessible solid reactants, such as hydroxides and oxides (Fig. 1D and E). While the mechanochemically-prepared BIFs exhibit significantly higher surface areas than the solvothermally-prepared counterparts, mechanochemistry allows for expanding this class of materials towards previously not reported Ag^+ nodes. The introduction of BIFs isostructural with those based on Li^+ or Cu^+ but comprising of Ag^+ ions, enables a periodic density-functional theory (DFT) evaluation of their stability. This reveals that switching to heavier elements as tetrahedral nodes improves the stability of sodalite topology (SOD) open BIFs with respect to close-packed diamondoid (dia) topology polymorphs.

As a first attempt at mechanochemically synthesis of BIFs, we targeted the synthesis of previously reported zni-topology LiB(**Im**)$_4$ and CuB(**Im**)$_4$ frameworks (Li-BIF-1 and Cu-BIF-1, respectively, Fig. 1A) using a salt exchange reaction between LiCl or CuCl with commercially available sodium tetrakis(imidazolyl)borate (Na[B(**Im**)$_4$]) (Fig. 2A). Milling of LiCl and Na[B(**Im**)$_4$] in a 1 : 1 stoichiometric ratio for up to 60 minutes led to the appearance of Bragg reflections consistent with the target Li-BIF-1 (CSD MOXJEP) and the anticipated NaCl byproduct. The reaction was, however, incomplete, as seen by X-ray reflections of Na[B(**Im**)$_4$] starting material. In order to improve reactant conversion, we explored liquid-assisted grinding (LAG), *i.e.* milling in the presence of a small amount of a liquid phase (measured by the liquid-to-solid ratio η[35] in the range of *ca.* 0–2 μL mg^{-1}). Using LAG conditions with acetonitrile (MeCN, 120 μL, η = 0.5 μL mg^{-1}) led to the complete disappearance of reactant X-ray reflections, concomitant with the formation of Li-BIF-1 alongside NaCl within 60 minutes.

Next, we explored an alternative synthesis approach, analogous to that previously used to form ZIFs and other MOFs: an acid–base reaction between a metal oxide or hydroxide and the acid form of the linker: tetrakis(imidazolato)boric acid, HB(**Im**)$_4$ (Fig. 3A).[36–40] Neat milling LiOH with one equivalent of HB(**Im**)$_4$ in a stainless steel milling assembly led to the partial formation of Li-BIF-1, as evidenced by PXRD analysis (see ESI†). Complete conversion of reactants into Li-BIF-1 was achieved in 60 minutes by LAG with MeCN (η = 0.25 μL mg^{-1}), as indicated by PXRD analysis (Fig. 3B–E), Fourier transform infrared attenuated total reflectance spectroscopy (FTIR-ATR), thermogravimetric analysis (TGA) in air, and analysis of metal content by inductively-coupled plasma mass spectrometry (ICP-MS) (see ESI†).

Neat milling of HB(**Im**)$_4$ with Cu_2O under similar conditions gave a largely non-crystalline material, as evidenced by PXRD (see ESI†). Switching to the ion- and liquid-assisted grinding (ILAG) methodology, in which the reactivity of a metal oxide is enhanced by a small amount of a weakly acidic ammonium salt, and which was introduced to prepare zinc and cadmium ZIFs from respective oxides,[37–40] enabled the synthesis of Cu-BIF-1 from Cu_2O. Specifically, PXRD analysis revealed complete disappearance of the oxide in samples obtained by ILAG with either MeOH or MeCN (η = 0.5 μL mg^{-1}) in the presence of NH_4NO_3 additive (5% by weight, see ESI†). Notably, achieving complete disappearance of Cu_2O reactant signals also required switching from stainless steel to a zirconia-based milling assembly, presumably due to more efficient energy delivery.[41] After washing with MeOH, the material was characterized by FTIR-ATR, TGA in air, and analysis of metal content by ICP-MS (see ESI†).

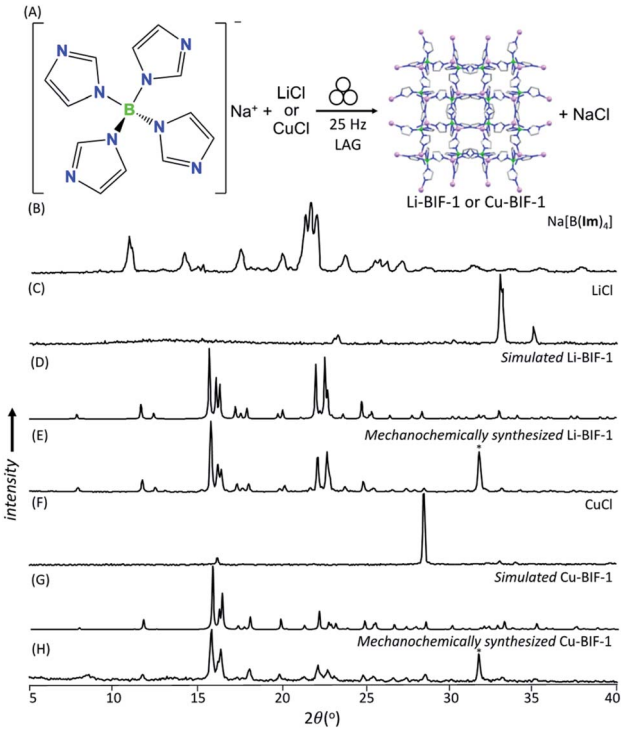

Fig. 2 (A) Reaction scheme for the mechanochemical synthesis of Li-BIF-1 by a salt metathesis strategy. Selected PXRD patterns for: (B) Na[B(Im)$_4$] (C) LiCl, (D) simulated Li-BIF-1 (CSD MOXJPEP) and (E) synthesized BIF-1-Li by LAG for 60 minutes with MeCN (η = 0.5 μL mg^{-1}), (F) CuCl, (G) simulated Cu-BIF-1 (CSD MOXJIT), and (H) synthesized BIF-1-Cu by LAG for 60 minutes with MeOH (η = 0.50 μL mg^{-1}). Asterisks denote NaCl, a byproduct of the metathesis reaction. (Fig. 2B–E, also see ESI†). The copper-based zni-CuB(Im)$_4$ (Cu-BIF-1) was readily obtained from CuCl within 60 minutes using similar LAG conditions. We also explored LAG with methanol (MeOH), revealing that the exchange reaction to form NaCl took place with both LiCl and CuCl starting materials. With LiCl, however, the PXRD pattern of the product could not be matched to known phases involving Li^+ and B(Im)$_4^-$ (see ESI†). With CuCl as a reactant, LAG with MeOH (η = 0.5 μL mg^{-1}) cleanly produced Cu-BIF-1 alongside NaCl (see ESI†).

Whereas both the metathesis and acid–base approaches can be used to mechanochemically generate Li- and Cu-BIF-1, the latter approach has a clear advantage of circumventing the formation of the NaCl byproduct. Consequently, in order to further the development of mechanochemical routes to other BIFs, we focused on the acid–base strategy. As next targets, we turned to MOFs based on tetrakis(2-methylimidazole)boric acid H[B(**Meim**)$_4$],[36] previously reported[32] to adopt either a non-porous diamondoid (dia) topology (BIF-2) or a microporous sodalite (SOD) topology (BIF-3) with either Li^+ or Cu^+ as nodes

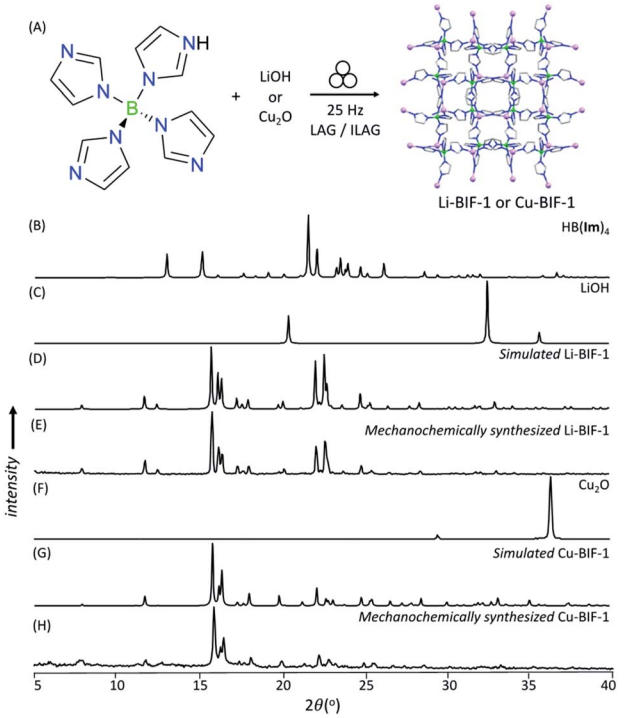

Fig. 3 (A) Reaction scheme for the mechanochemical synthesis of Li-BIF-1 using the acid–base strategy. Selected PXRD patterns for: (B) H[B(**Im**)$_4$] (C) LiOH, (D) simulated Li-BIF-1 (CSD MOXJPEP), (E) synthesized BIF-1-Li by LAG for 60 minutes with MeCN (η = 0.25 μL mg^{-1}), (F) Cu_2O, (G) simulated Cu-BIF-1 (CSD MOXJIT), and (H) synthesized Cu-BIF-1 by ILAG for 60 minutes with MeOH (η = 0.50 μL mg^{-1}) and NH_4NO_3 additive (5% by weight).

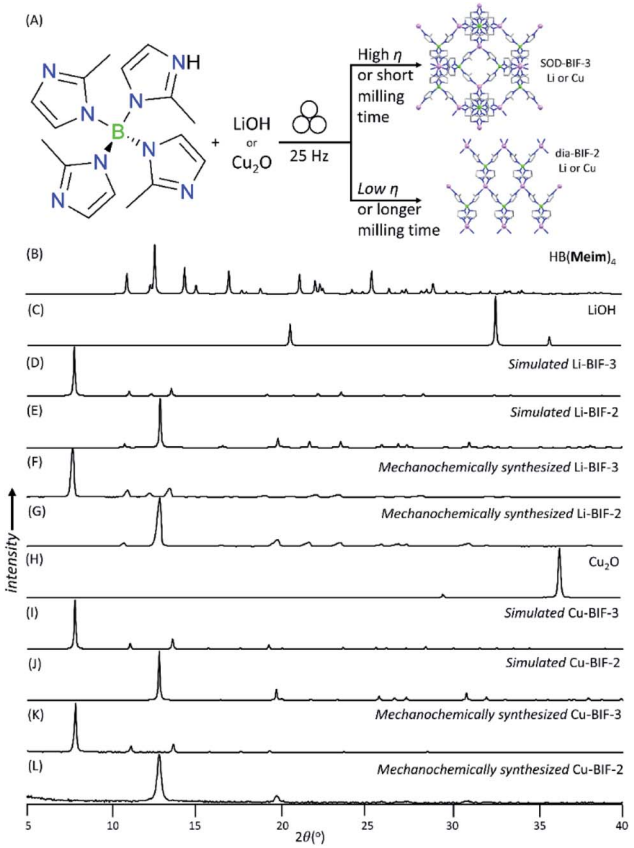

Fig. 4 (A) Reaction scheme for the mechanochemical synthesis of Li-BIF-3. Comparison of selected PXRD patterns for the synthesis of Li-BIF-2 and Li-BIF-3: (B) H[B(**Meim**)$_4$] reactant; (C) LiOH reactant; (D) simulated for Li-BIF-3 (CSD MUCLOM); (E) simulated for Li-BIF-2 (CSD MOXKUG); (F) Li-BIF-3 mechanochemically synthesized by LAG for 60 minutes with a 1 : 3 by volume mixture of **amb** and MeCN (η = 1 μL mg^{-1}); and (G) Li-BIF-2 mechanochemically synthesized by LAG for 60 minutes with a 1 : 3 by volume mixture of **amb** and MeCN (η = 0.5 μL mg^{-1}). Comparison of selected PXRD patterns for the synthesis of Cu-BIF-2 and Li-BIF-3: (H) Cu_2O; (I) Cu-BIF-3 (CSD MOXJOZ); (J) Cu-BIF-2 (CSD MUCLIG); (K) Cu-BIF-3 mechanochemically synthesised by ILAG for 60 minutes using NH_4NO_3 ionic additive (5% by weight) and MeOH (η = 1 μL mg^{-1}); and (L) mechanochemically synthesised Cu-BIF-2 by ILAG for 90 minutes using NH_4NO_3 ionic additive (5% by weight) and MeOH (η = 0.5 μL mg^{-1}).

(Fig. 4). Attempts to selectively synthesize either Li-BIF-2 or Li-BIF-3 by neat milling or LAG (using MeOH or MeCN as liquid additives) with LiOH and a stoichiometric amount of HB(**Meim**)$_4$ were not successful. Exploration of different milling times and η-values produced only mixtures of residual reactants with Li-BIF-2, Li-BIF-3, and/or not yet identified phases (see ESI†). Consequently, we explored milling in the presence of 2-aminobutanol (**amb**), which is a ubiquitous component of solvent systems used in the solvothermal syntheses of BIFs.[32,33] Gratifyingly, using a mixture of **amb** and MeCN in a 1 : 3 ratio by volume as the milling liquid led to an effective strategy for the selective synthesis of both the dia-topology Li-BIF-2 (CSD code MOXKUG), and the SOD-topology Li-BIF-3 (CSD code MUCLOM).§ The selective formation of phase-pure samples of Li-BIF-2 and Li-BIF-3 was confirmed by PXRD analysis, which revealed an excellent match to diffractograms simulated based on the previously reported structures (Fig. 4B–G). Systematic exploration of reaction conditions, including time (between 15 and 60 minutes) and η value (between 0.25 and 1 μL mg^{-1}) revealed that the open framework Li-BIF-3 is readily obtained at η either 0.75 or 1 μL mg^{-1} after milling for 45 minutes or longer (Fig. 4B–G, also see ESI†).‡ Lower η-values of 0.25 and 0.5 μL mg^{-1} preferred the formation of the dia-topology Li-BIF-2, which was obtained as a phase-pure material upon 60 minutes milling at η = 0.5 μL mg^{-1}, following the initial appearance of a yet unidentified intermediate. The preferred formation of Li-BIF-2 at lower η-values is consistent with our previous observations that lower amounts of liquid promote mechanochemical formation of denser MOF polymorphs.[37]

Samples of both Li-BIF-2 and Li-BIF-3 after washing with MeCN were further characterized by FTIR-ATR, TGA in air, and analysis of metal content by ICP-MS (see ESI†). Nitrogen sorption measurement on the mechanochemically obtained Li-BIF-3, after washing with MeCN and evacuation at 85 °C, revealed a highly microporous material with a Brunauer–Emmett–Teller (BET) surface area of 1010 m^2 g^{-1} (Table 1 and Fig. 5A), which is close to the value expected from the crystal structure of the material (1200 m^2 g^{-1}, Table 1).[32] For direct comparison with previous work,[32] we also calculated the Langmuir surface area, revealing an almost 40% increase (1060 m^2 g^{-1}) compared to

Table 1 Experimental Brunauer–Emmett–Teller (BET) and Langmuir surface area (in $m^2\ g^{-1}$) of mechanochemically synthesized SOD-topology BIFs, compared to previously measured and theoretically calculated values, along with average particle sizes (in nm) established by SEM and calculated energies (in eV) for all Li-, Cu-, and Ag-BIF polymorphs. The difference between calculated energies for SOD- and dia-polymorphs in each system is given as ΔE (in kJ mol^{-1})

Material	Surface area ($m^2\ g^{-1}$)				Particle size[b] (nm)	Electronic energy per formula unit (eV)	ΔE (kJ mol^{-1})
	Mechanochemical, BET	Mechanochemical, Langmuir	Prior work, Langmuir [32]	Theoretical[a]			
dia-Li-BIF-2	—	—	—	—	—	−2679.174	14.25
SOD-Li-BIF-3	1010	1060	762.5	1200	217 ($n = 24$)	−2679.026	
dia-Cu-BIF-2	—	—	—	—	—	−3417.091	9.67
SOD-Cu-BIF-3	935	1196	182.3	1100	611 ($n = 500$)	−3416.991	
dia-Ag-BIF-2	—	—	—	—	—	−4738.959	8.66
SOD-Ag-BIF-3	1020	1205	—	1170	500 ($n = 25$)	−4738.869	

[a] Calculated using MOF Explorer (see ESI). [b] Determined from SEM measurements, where n corresponds to number of particles observed.

samples made solvothermally (762.5 $m^2\ g^{-1}$) (Table 1). Analysis of Li-BIF-3 by scanning electron microscopy (SEM) revealed particles with sizes of hundreds of nanometres, forming larger aggregates several micrometres across (Fig. 5A, inset).

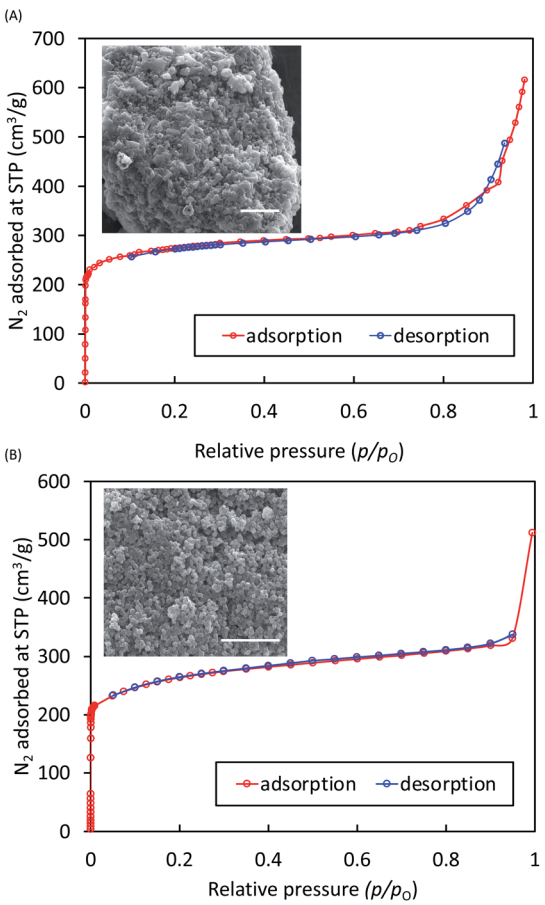

Fig. 5 BET adsorption plots for: (A) Li-BIF-3, showing a surface area of 1010 $m^2\ g^{-1}$ and (B) Cu-BIF-3, showing a surface area of 935 $m^2\ g^{-1}$. The insets in (A) and (B) are representative SEM images of the mechanochemically prepared BIF samples, with scale bars corresponding to 4 μm and 5 μm shown in white.

The analogous copper(I)-based BIF-2 and BIF-3 frameworks were readily accessible by ILAG, by controlling the volume of the liquid additive and milling time (Fig. 4H–L, also see ESI†). Similarly to our previous studies of ZIFs,[17,24,37,39] increased milling times preferred the formation of the close-packed polymorph, dia-topology Cu-BIF-2. While the PXRD pattern of the reaction mixture after 60 minutes ILAG with MeOH ($\eta = 0.5$ μL mg^{-1}) and NH_4NO_3 (5% wt/wt) indicated the presence of the SOD-topology Cu-BIF-3, longer milling led to the appearance of the dia-phase (see ESI†). The materials were identified through comparison of experimental PXRD patterns to those simulated from published structures (CSD codes MUCLIG and MOXJOZ for Cu-BIF-2 and Cu-BIF-3, respectively).[32] Quantitative synthesis of Cu-BIF-2 from Cu_2O was readily accomplished by ILAG for 90 minutes (Fig. 4H–L). Following washing and drying, the products were characterized by PXRD, FTIR-ATR, TGA in air and ICP-MS elemental analysis of metal content.

In order to achieve the synthesis of phase-pure microporous Cu-BIF-3, reaction conditions were modified by increasing η to 1 μL mg^{-1}. This modification enabled the reproducible and quantitative synthesis of Cu-BIF-3 in 60 minutes milling (Fig. 4H–L), confirmed by PXRD, FTIR-ATR, TGA and elemental analysis of metal content (see ESI†). Analyses by SEM and nitrogen sorption were performed on the mechanochemical product after washing and drying *in vacuo* at 85 °C, revealing that the sample consists of sub-micron particles and exhibits a high BET surface area of 935 $m^2\ g^{-1}$, which is close to the theoretically expected value of 1100 $m^2\ g^{-1}$ (Table 1 and Fig. 5B). To enable direct comparison with previously reported work,[32] we also calculated the Langmuir surface area, revealing a 7-fold increase (1196 $m^2\ g^{-1}$) compared to samples made solvothermally (182.3 $m^2\ g^{-1}$) (Table 1).

To verify whether the improvement in surface area was attributable to the mechanochemical synthesis or the different activation procedure, a sample of Cu-BIF-3 was synthesized according to the published solvothermal methodology and activated in the same way as the mechanochemically prepared

material. The resulting Cu-BIF-3 exhibited a BET surface area of 616 $m^2\ g^{-1}$ (see ESI†), *i.e.* 34% lower compared to the mechanochemically synthesized sample, illustrating a clear benefit of mechanochemistry in providing a simpler, more efficient synthesis, as well as materials of improved porosity.[32,42]

The mechanochemical approaches to Li- and Cu-based BIFs are surprisingly simple compared to previously reported solvothermal methods,[32,33,42] not only avoiding bulk solvents and high temperatures (85 °C for Li-based, 120 °C for Cu-based BIFs), but also enabling the use of simple, easily handled solids LiOH and Cu_2O as starting materials compared to, for example, *n*-BuLi.[42] Notably, while the reported solvothermal synthesis of these materials also requires the use of **amb** for the preparation of both Li- and Cu-BIFs, the use mechanochemical conditions enabled **amb**-free synthesis of copper-based BIFs. Such simplifications of the synthetic procedure encouraged us to explore the possibility to extend this family of materials towards previously not reported silver(I) derivatives.

As a starting material for the synthesis of Ag(I)-based BIFs we focused on Ag_2CO_3, generated *in situ* from readily accessible $AgNO_3$ and K_2CO_3. One-pot milling reaction of HB(**Meim**)$_4$, $AgNO_3$, and K_2CO_3 in the respective stoichiometric ratios 1 : 1 : 1/2, using MeCN as the milling additive (η = 0.25 μL mg^{-1}) readily produced the targeted AgB(**Meim**)$_4$ material along with the side product KNO_3 (Fig. 5, also see ESI†). Specifically, analysis of the reaction mixtures by PXRD revealed that, similar to the lithium and copper(I) analogues,[32] the silver-based BIF appears in two polymorphs which could be selectively synthesized by varying the milling time. The BIF products were readily separated from the KNO_3 by-product after sequential washing with cold MeOH and acetone, and their respective structures were further validated by structure determination from PXRD data measured on washed and dried materials.

Specifically, milling for 30 minutes led to the formation of a material (Ag-BIF-3) which, based on PXRD analysis, was isostructural to the SOD-topology Li-BIF-3 and Cu-BIF-3. Consequently, the crystal structure of Ag-BIF-3 (Fig. 5A) was determined through Rietveld refinement of a structural model based on the Cu-BIF-3 structure, in which the copper(I) sites have been replaced by Ag(I), giving rise to a cubic unit cell (space group $P\bar{4}3n$ as in the analogous Cu-BIF-3 and Li-BIF-3 structures) with a = 16.6659(3) Å. Composition of Ag-BIF-3 was verified by TGA/DSC and elemental analysis of metal content (see ESI†). The microporous nature of the material was confirmed by N_2 sorption analysis, which revealed a high BET surface area of 1020 $m^2\ g^{-1}$. Sample analysis by SEM revealed dense aggregates of particles, with sizes below 100 nm (Fig. 5). The ^{13}C cross-polarisation magic angle spinning (CP-MAS) solid-state nuclear magnetic resonance (ssNMR) spectrum of Ag-BIF-3 was consistent with the crystal structure, revealing three signals in the imidazolate region 100–160 ppm and the $-CH_3$ group signal at ~16 ppm (Fig. 6).

Milling for 60 minutes under otherwise identical conditions led to a material whose PXRD pattern was very similar, but not identical, to that of dia-topology Li-BIF-2 and Cu-BIF-2 materials, with additional Bragg reflections indicating possible lower symmetry. The structure of this material (Fig. 6B) was determined by simulated annealing structure solution from PXRD data, revealing a monoclinic (space group $P2_1$) unit cell with a = 7.5198(4) Å, b = 16.3763(9) Å, c = 7.5876(4) Å and β = 90.136(6)o. In contrast to structures of Li-BIF-2 and Cu-BIF-2, which all exhibited one symmetrically independent **Meim**$^-$ ligand in a tetragonal $I\bar{4}$ space group, the structure of Ag-BIF-3 displays each tetrahedral node surrounded by four symmetrically non-equivalent imidazolate ligands. This much higher multiplicity is clearly reflected by the ssNMR spectrum of the material, validating the structure (Fig. 6). The composition of the material was similarly confirmed by TGA and by elemental analysis of the metal content (see ESI†). For both Ag-BIF-2 and Ag-BIF-3 the measured ^{13}C ssNMR chemical shifts were consistent with those calculated from the herein determined crystal structures (Fig. 6D–G). Notably, while materials based on silver(I) ions are often expected to be light sensitive, the herein reported Ag-BIF-2 and Ag-BIF-3 both appeared unchanged following six months exposure storage in a transparent vial on the bench.

The crystal structures of Li-, Cu- and Ag-based BIFs provide a unique opportunity to evaluate the effect of changes in the metal node on the relative stability of BIF polymorphs with SOD- and dia-topology across three metals.[43–45] The calculations were done using CASTEP plane-wave density-functional theory (DFT)[46] code. The previously published crystal structures of Li- and Cu-BIFs with **Meim**$^-$ linkers, as well as the structures of Ag-BIFs herein determined, were geometry-optimized using the PBE[47] functional combined with many-body dispersion (MBD*)[48–50] correction scheme. The PBE + MBD* approach has previously shown excellent agreement with experimental calorimetric measurements of ZIF polymorphs,[24] therefore we expected the same approach to perform reliably for the structures of BIFs. In addition to calculating the relative energies of SOD- and dia-polymorphs, we have performed Gauge Including Projector Augmented Waves (GIPAW)[51] simulation of the solid-state NMR spectra of Ag-BIFs to compare the simulated spectra with their experimental counterparts, confirming the low symmetry Ag-BIF-2 structure derived from PXRD data (Fig. 6D–G).

Comparison of calculated energies reveals that increasing the atomic number of the metal node results in increased stabilization of the SOD-topology open framework with respect to the close-packed dia-polymorph. The energy differences (ΔE) between SOD- and dia-topology polymorphs for each pair of Li-, Cu-, and Ag-based frameworks are shown in Table 1. Specifically, whereas Li-BIF-3 structure is calculated to be *ca.* 14 kJ mol^{-1} less stable compared to its dia-counterpart, the corresponding differences for Cu-BIF-3 and Ag-BIF-3 are calculated to be considerably smaller, at 9.7 kJ mol^{-1} and 8.7 kJ mol^{-1}, respectively. The calculated energies are in a similar range to the calculated (15.2 kJ mol^{-1}) and measured (10.6 kJ mol^{-1}) ones for the analogous zinc-based ZIFs, indicating that switching between transition metal and main group-based nodes, or switching between using only a divalent node and a combination of monovalent and trivalent nodes, does not significantly influence the difference in stability of SOD- and dia-topology frameworks. The improvement in the relative

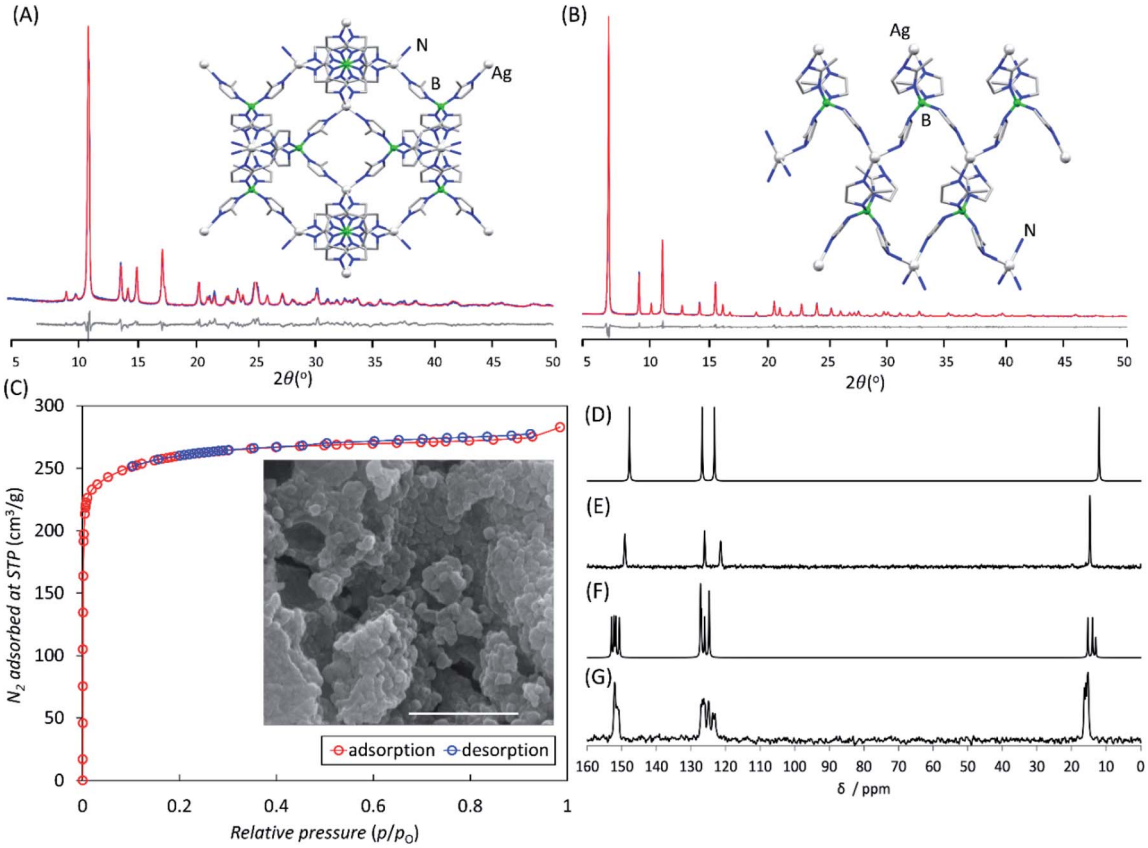

Fig. 6 (A) Rietveld refinement of Ag-BIF-3 with difference plot shown in grey. (B) Rietveld refinement of Ag-BIF-2 with difference plot shown in grey. (C) BET adsorption plot Ag-BIF-3 showing a surface area of 1020 $m^2\ g^{-1}$ and a SEM image of a representative sample (scale-bar 1 μm). Comparison of measured and simulated ^{13}C CP-MA ssNMR spectra for silver-based BIFs: (D) calculated for Ag-BIF-3, (E) measured for Ag-BIF-3, (F) calculated for Ag-BIF-2 and (G) measured for Ag-BIF-2.

stability of open BIF structure upon switching from Li^+ to Cu^+ and Ag^+ nodes is notable, considering the recent interest in the development of MOFs based on heavy-atom nodes.[52–54]

The simulated ssNMR spectra of Ag-BIF-2 and Ag-BIF-3 showed excellent agreement with the experiment (Fig. 6) in terms of overall chemical shift and the number of distinct NMR signals arising from the crystallographic symmetry. The spectrum of the SOD polymorph is consistent with a single symmetrically unique **Meim**$^-$ linker, while the signal splitting found in the spectrum of the dia-polymorph corresponds to four distinct 2-methylimidazolate units. The NMR simulation fully supports the structural models derived from PXRD data, with calculated chemical shifts underlining the accuracy of the herein used theoretical approach.

Conclusions

In summary, we have shown that the application of mechanochemical methodologies can greatly simplify the synthesis of zeolitic boron imidazolate frameworks, providing a rapid, room-temperature approach to this class of materials. Contrary to previously reported materials obtained by solvothermal synthesis, the open framework SOD-topology BIFs made mechanochemically show higher surface areas, that are very close to the theoretically calculated ones. The use of mechanochemistry also expanded the scope of the zeolitic BIF class of materials, by enabling the synthesis of previously not reported silver-based systems.¶ Theoretical investigation of isostructural BIFs based on Li^+, Cu^+ and Ag^+ reveals that the use of increasingly heavier tetrahedral metal nodes leads to the stabilization of open-framework SOD-topology structure with respect to the corresponding close-packed dia polymorph. Overall, the presented results and synthetic methodologies should provide simpler, faster access to an intriguing, but so far poorly developed, class of ultralight zeolitic MOFs.

Data availability

Details of experimental and theoretical procedures, and selected PXRD, TGA, FTIR-ATR, ICP-MS, and nitrogen sorption data are provided as part of the ESI.† Crystallographic data for compounds BIF-2-Ag, BIF-3-Ag and [H**amb**$^+$][B(**Meim**)$_4^-$]·$2H_2O$ have been deposited at the Cambridge Crystallographic Data Centre (CCDC) under deposition codes 2081806, 2081807, and 2084944, respectively.

Author contributions

All authors have contributed to the writing of this manuscript. Development of mechanochemical synthesis procedures and

characterization of new materials was performed by C. B. L., J. G. C., J.-L. D. The materials characterization was done by H. M. T., A. J. H., and theoretical studies by M. A. The research was organized and coordinated by T. F.

Conflicts of interest

There are no conflicts to declare.

Acknowledgements

We acknowledge support of NSERC Discovery Grant (RGPIN-2017-06467), Discovery Accelerator Award (RGPAS 507837-17), Strategic Grant (STPGP 521582-18), and PGS-D Scholarship (to C. B. L.). MA thanks the National Science Center of Poland (NCN) for the support *via* SONATA grant (2018/31/D/ST5/03619). We also thank PL-Grid for access to the Prometheus supercomputer. Dr Robin S. Stein is acknowledged for help in acquiring NMR data. Anna Jung of McGill Department of Earth and Planetary Sciences for ICP-MS measurements, and Dr David Liu of the Facility for Electron Microscopy Research (FEMR), McGill University, for SEM imaging.

Notes and references

§ The use of **amb** in the synthesis of BIFs has not been explained.[32–34] Based on the herein reported mechanochemical studies, we believe **amb** provides a means to increase the reactivity of the HB(**Meim**)$_4$ ligand, potentially through salt formation, and also hinders the re-arrangement of open-structure Li-BIF-3 into Li-BIF-2. For example, 30 minutes milling of LiOH and HB(**Meim**)$_4$ in presence of MeCN at $\eta = 1$ μL mg^{-1} leads to a mixture of Li-BIF-2, Li-BIF-3 and HB(**Meim**)$_4$, which is evident by PXRD analysis. Milling in presence of a mixture of MeCN and **amb** (3 : 1 by volume, $\eta = 1$ μL mg^{-1}), however, leads to complete disappearance of PXRD signals of HB(**Meim**)$_4$, and Li-BIF-3 as the only product.

‡ In some cases during screening reaction conditions, the PXRD pattern of the product exhibited Bragg reflections that could not be assigned to neither Li-BIF-2, LiBIF-3, or any of the reactants. These were subsequently found to result from the parasitic formation of the hydrated salt [H**amb**$^+$][B(**Meim**)$_4^-$]·2H$_2$O, whose structure was determined from separately prepared single crystals (see ESI,† CCDC deposition code 2084944). The formation of [H**amb**$^+$][B(**Meim**)$_4^-$]·2H$_2$O, however, can be avoided by drying both MeCN and **amb** over molecular sieves before use.

¶ Preliminary attempts to synthesize the Ag-BIFs from acetonitrile solution, using the methodology that was reported for Cu-BIF-3, gave a yet unidentified material. Replacing the solvent with MeOH gave a mixture of phases containing Ag-BIF-2, along with significant amount of metallic silver, evident by the black color of the material.

1 S. L. James, C. J. Adams, C. Bolm, D. Braga, P. Collier, T. Friščić, F. Grepioni, K. D. M. Harris, G. Hyett, W. Jones, A. Krebs, J. Mack, L. Maini, A. G. Orpen, I. P. Parkin, W. C. Shearouse, J. W. Steed and D. C. Waddell, *Chem. Soc. Rev.*, 2012, **41**, 413–447.
2 T. Friščić, C. Mottillo and H. M. Titi, *Angew. Chem., Int. Ed.*, 2020, **13**, 1018–1029.
3 N. R. Rightmire and T. P. Hanusa, *Dalton Trans.*, 2016, **45**, 2352–2362.
4 E. Boldyreva, *Chem. Soc. Rev.*, 2013, **42**, 7719–7738.
5 A. Porcheddu, E. Colacino, L. De Luca and F. Delogu, *ACS Catal.*, 2020, **10**, 8344–8394.
6 J. M. Andersen and J. Mack, *Chem. Sci.*, 2017, **8**, 5447–5453.
7 C. Bolm and J. G. Hernández, *Angew. Chem., Int. Ed.*, 2019, **58**, 3285–3299.
8 P. Baláž, M. Achimovičová, M. Baláž, P. Billik, Z. Cherkezova-Zheleva, J. M. Criado, F. Delogu, E. Dutková, E. Gaffet, F. J. Gotor, R. Kumar, I. Mitov, T. Rojac, M. Senna, A. Streletskii and K. Wieczorek-Ciurowa, *Chem. Soc. Rev.*, 2013, **42**, 7571–7637.
9 B. G. Fiss, N.-N. Vu, G. Douglas, T.-O. Do, T. Friščić and A. Moores, *ACS Sustain. Chem. Eng.*, 2020, **8**, 12014–12024.
10 D. Prochowicz, M. Saski, P. Yadav, M. Grätzel and J. Lewiński, *Acc. Chem. Res.*, 2019, **52**, 3233–3243.
11 D. DeSantis, J. A. Mason, B. D. James, C. Houchins, J. R. Long and M. Veenstra, *Energy Fuels*, 2017, **31**, 2024–2032.
12 T. Stolar and K. Užarević, *CrystEngComm*, 2020, **22**, 4511–4525.
13 R. Riccò, O. Linder-Patton, K. Sumida, M. J. Styles, K. Liang, H. Amenitsch, C. J. Doonan and P. Falcaro, *Chem. Mater.*, 2018, **30**, 5630–5638.
14 D. Crawford, J. Casaban, R. Haydon, N. Giri, T. McNally and L. S. James, *Chem. Sci.*, 2015, **6**, 1645–1649.
15 K. Užarević, T. C. Wang, S. Y. Moon, A. M. Fidelli, J. T. Hupp, O. K. Farha and T. Friščić, *Chem. Commun.*, 2016, **52**, 2133–2136.
16 A. D. Katsenis, A. Puškarić, V. Štrukil, C. Mottillo, P. A. Julien, K. Užarević, M. H. Pham, T. O. Do, S. A. J. Kimber, P. Lazić, O. Magdysyuk, R. E. Dinnebier, I. Halasz and T. Friščić, *Nat. Commun.*, 2015, **6**, 6662.
17 M. Arhangelskis, A. D. Katsenis, N. Novendra, Z. Akimbekov, D. Gandrath, J. M. Marrett, G. Ayoub, A. J. Morris, O. K. Farha, T. Friščić and A. Navrotsky, *Chem. Mater.*, 2019, **31**, 3777–3783.
18 W. Xu, H. Chen, K. Jie, Z. Yang, T. Li and S. Dai, *Angew. Chem., Int. Ed.*, 2019, **58**, 5018–5022.
19 D. E. Crawford and J. Casaban, *Adv. Mater.*, 2016, **28**, 5747–5754.
20 A. A. L. Michalchuk, K. S. Hope, S. R. Kennedy, M. V. Blanco, E. V. Boldyreva and C. R. Pulham, *Chem. Commun.*, 2018, **54**, 4033–4036.
21 H. M. Titi, J.-L. Do, A. J. Howarth, K. Nagapudi and T. Friščić, *Chem. Sci.*, 2020, **11**, 7578–7584.
22 P. A. Julien, C. Mottillo and T. Friščić, *Green Chem.*, 2017, **19**, 2729–2747.
23 T. Friščić and L. Fábián, *CrystEngComm*, 2009, **11**, 743–745.
24 Z. Akimbekov, A. D. Katsenis, G. P. Nagabhushana, G. Ayoub, M. Arhangelskis, A. J. Morris, T. Friščić and A. Navrotsky, *J. Am. Chem. Soc.*, 2017, **139**, 7952–7957.
25 N. Novendra, J. M. Marrett, A. D. Katsenis, H. M. Titi, M. Arhangelskis, T. Friščić and A. Navrotsky, *J. Am. Chem. Soc.*, 2020, **142**, 21720–21729.
26 M. Klimakow, P. Klobes, A. F. Thünemann, K. Rademann and F. Emmerling, *Chem. Mater.*, 2010, **22**, 5216–5221.
27 K. Užarević, T. C. Wang, S.-Y. Moon, A. M. Fidelli, J. T. Hupp, O. K. Farha and T. Friščić, *Chem. Commun.*, 2016, **52**, 2133–2136.
28 B. Karadeniz, A. J. Howarth, T. Stolar, T. Islamoglu, I. Dejanovic, M. Tireli, M. C. Wasson, S.-Y. Moon,

O. K. Farha, T. Friščić and K. Užarević, *ACS Sustainable Chem. Eng.*, 2018, **6**, 15841–15849.
29 P. A. Julien, K. Užarević, A. D. Katsenis, S. A. J. Kimber, T. Wang, O. K. Farha, Y. Zhang, J. Casaban, L. S. Germann, M. Etter, R. E. Dinnebier, S. L. James, I. Halasz and T. Friščić, *J. Am. Chem. Soc.*, 2016, **138**, 2929–2932.
30 K. S. Park, Z. Ni, A. P. Côte, J. Y. Choi, R. Huang, F. J. Uribe-Romo, H. K. Chae, M. O'Keeffe and O. M. Yaghi, *Proc. Natl. Acad. Sci. U.S.A.*, 2006, **103**, 10186–10191.
31 J.-P. Zhang, Y.-B. Zhang, J.-B. Lin and X.-. Chen, *Chem. Rev.*, 2012, **112**, 1001–1033.
32 J. Zhang, T. Wu, C. Zhou, S. Chen, P. Feng and X. Bu, *Angew. Chem., Int. Ed.*, 2009, **48**, 2542–2545.
33 T. Wu, J. Zhang, C. Zhou, L. Wang, X. Bu and P. Feng, *J. Am. Chem. Soc.*, 2009, **131**, 6111–6113.
34 V. I. Isaeva, K. E. Papathanasiou and L. M. Kustov, *Crystals*, 2020, **10**, 617.
35 T. Friščić, S. L. Childs, S. A. A. Rizvi and W. Jones, *CrystEngComm*, 2009, **11**, 418–426.
36 P. J. Bailey, D. Lorono-Gonzales, C. McCormack, F. Millican, S. Parsons, R. Pfeifer, P. P. Pinho, F. Rudolphi and A. Sanchez Perucha, *Chem. Eur. J.*, 2006, **12**, 5293–5300.
37 T. Friščić, I. Halasz, P. J. Beldon, A. M. Belenguer, F. Adams, S. A. J. Kimber, V. Honkimäki and R. E. Dinnebier, *Nat. Chem.*, 2013, **5**, 66–73.
38 T. Friščić, D. G. Reid, I. Halasz, R. S. Stein, R. E. Dinnebier and M. J. Duer, *Angew. Chem., Int. Ed.*, 2010, **49**, 712–715.
39 P. J. Beldon, L. F. Fabain, R. S. Stein, A. Thirumurugan, A. K. Cheetham and T. Friščić, *Angew. Chem., Int. Ed.*, 2010, **49**, 9640–9643.
40 C. A. O'Keeffe, C. Mottillo, J. Vainauskas, L. Fábián, T. Friščić and R. W. Schurko, *Chem. Mater.*, 2020, **32**, 4273–4281.
41 L. S. Germann, M. Arhangelskis, M. Etter, R. E. Dinnebier and T. Friščić, *Chem. Sci.*, 2020, **11**, 10092–10100.
42 The previously reported synthesis of Li-BIF-3 involves the use of HB(**Meim**)$_4$ with *n*-BuLi, in a mixture of **amb** and acetonitrile at a temperature of 85 °C, for 5 days. The reported synthesis of Cu-BIF-3 in solution is achieved from HB(**Meim**)$_4$, CuI, and **amb** in acetonitrile solution after 5 days at 120 °C (ref. 32).
43 R. Galvelis, B. Slater, A. K. Cheetham and C. Mellot-Draznieks, *CrystEngComm*, 2012, **14**, 374–378.
44 C. Mellot-Draznieks and B. Kerkeni, *Mol. Simul.*, 2014, **40**, 25–32.
45 I. A. Baburin and S. Leoni, *J. Mater. Chem.*, 2012, **22**, 10152–10154.
46 S. J. Clark, M. D. Segall, C. J. Pickard, P. J. Hasnip, M. I. J. Probert, K. Refson and M. C. Payne, *Z. Krist.*, 2009, **220**, 567–570.
47 A. Vela, J. C. Pacheco-Kato, J. L. Gázquez, J. M. del Campo and S. B. Trickey, *J. Chem. Phys.*, 2012, **136**, 144115.
48 A. Tkatchenko, R. A. DiStasio, R. Car and M. Scheffler, *Phys. Rev. Lett.*, 2012, **108**, 236402.
49 A. Ambrosetti, A. M. Reilly, R. A. DiStasio and A. Tkatchenko, *J. Chem. Phys.*, 2014, **140**, 18A508.
50 A. M. Reilly and A. Tkatchenko, *Chem. Sci.*, 2015, **6**, 3289–3301.
51 J. R. Yates, C. J. Pickard and F. Mauri, *Phys. Rev. B*, 2007, **76**, 024401.
52 K. P. Carter, J. A. Ridenour, M. Kalaj and C. L. Cahill, *Chem. Eur. J.*, 2019, **25**, 7114–7118.
53 S. E. Gilson, P. Li, J. E. S. Szymanowski, J. White, D. Ray, L. Gagliardi, O. K. Farha and P. C. Burns, *J. Am. Chem. Soc.*, 2019, **141**, 11842–11846.
54 I. R. Speight, I. Huskic, M. Arhangelskis, H. M. Titi, R. S. Stein, T. P. Hanusa and T. Friščić, *Chem. Eur. J.*, 2020, **26**, 1811–1818.